

# QCD-Factorization of inclusive $B$ decays and $|V_{ub}|$ \*

CLNS 04/1889

Björn O. Lange <sup>a</sup>

<sup>a</sup>Institute for High-Energy Phenomenology, Newman Laboratory for High-Energy Physics, Cornell University, Ithaca, NY 14853, U.S.A.

Recent progress in the theoretical description of inclusive  $B \rightarrow X_u l^- \bar{\nu}$  decays in the shape-function region is reported. Finite moments of the shape function are related to HQET parameters. Event fractions for several experimental cuts are presented, with a particular emphasis on the hadronic variable  $P_+ = E_H - |\vec{P}_H|$ . The aim of this talk is to introduce the  $P_+$  spectrum, to compare it to the hadronic invariant mass spectrum and the charged-lepton energy spectrum, and to study the prospect of evaluating  $|V_{ub}|$  in the presence of a large background from  $B \rightarrow X_c$  decays.

## 1. INTRODUCTION

Studies of both exclusive and inclusive semileptonic decays of the  $B$  meson can be used to extract the magnitude of the CKM matrix element  $|V_{ub}|$ . Both methods require some input from theory. Because the exclusive modes suffer from large form-factor uncertainties, the determination from inclusive  $B \rightarrow X_u l^- \bar{\nu}$  decays are theoretically favored. The overall relative uncertainty on  $|V_{ub}|$  measurements is currently about 15% [1], and there is hope for a significant reduction of the dominant theoretical errors in the future. The main problem in the computation of the relevant quantities is that it requires a framework which includes a systematic treatment of both perturbative corrections (including Sudakov resummation) and non-perturbative effects (shape function). Much progress in QCD-Factorization of inclusive  $B$  decays has been made in the past several months [2–4], and the aforementioned problem is now understood using a sophisticated effective field theory machinery. The main ingredients are Soft-Collinear Effective Theory (SCET) [5–7], Heavy-Quark Effective Theory (HQET) [8], and Renormalization-Group (RG) evolution of bilocal operators on the light cone [9].

Let us begin by discussing the kinematic setup used in the description of a typical  $B \rightarrow X_u l^- \bar{\nu}$

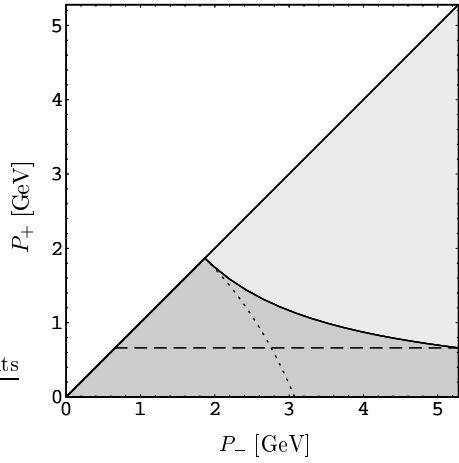


Figure 1. Hadronic phase space in the light-cone variables  $P_+$  and  $P_-$ . The dark gray area is free of  $B \rightarrow X_c$  background events, which occur in the light gray wedge above. For an explanation of the dashed and dotted curve, see the text.

event. The momentum of the hadronic  $X_u$  system is denoted by  $P_H^\mu$ , and we work in the rest frame of the  $B$  meson. It is useful to describe the hadronic phase space in the variables  $P_+ = E_H - |\vec{P}_H|$  and  $P_- = E_H + |\vec{P}_H|$ , in which it takes the simple form of a triangle (neglecting the pion mass)

$$0 \leq P_+ \leq P_- \leq M_B . \quad (1)$$

The phase space is depicted in Figure 1. The use

\*Talk presented at the Sixth International Conference on Hyperons, Charm and Beauty Hadrons, IIT, Chicago, June 27–July 3 2004.

of the light-cone variables  $P_+$  and  $P_-$  makes it easy to interpret an event (a point) in this picture: the region of low recoil is along the diagonal, while an event with a maximally recoiling  $X_u$  is located on the right. Events with final-state hadronic invariant masses larger than  $M_D$  are located in the light-gray wedge in the upper part of the Figure, since  $M_X^2 = P_+ P_-$ . The dark-gray region underneath is free of the  $B \rightarrow X_c$  background, which is about 60 times larger than the  $B \rightarrow X_u$  signal.

There are many possibilities to eliminate the background by cutting on kinematic variables. Let us briefly mention a few of them. Clearly a cut on  $M_X^2 \leq M_D^2$  is the “ideal” separator, denoted as a solid line in Figure 1. The dashed horizontal line is located at  $P_+ = M_D^2/M_B$ , which marks an alternative way of eliminating charm events. A cut on the charged-lepton energy  $E_l \geq (M_B^2 - M_D^2)/2M_B$  samples the same hadronic phase space as a cut on  $P_+ \leq M_D^2/M_B$ . However, it contains far fewer events. Finally, a cut on the dilepton momentum squares  $q^2 \leq (M_B - M_D)^2$  leads to the area underneath the dotted line.

The phase space is most densely populated in the “shape-function region” of large  $P_- \sim O(M_B)$  and small  $P_+ \sim O(\Lambda_{\text{QCD}})$ . In order to determine  $|V_{ub}|$  from this inclusive decay mode it is necessary to know what fractions of events survive the various experimental cuts. In this talk we report on progress to answer this question. In addition, we advertise cutting on  $P_+$  as an efficient method for future  $|V_{ub}|$  determinations. To this end we study the advantages and disadvantages of this method over comparable ones, in particular the “ideal separator”  $M_X$ .

## 2. FACTORIZATION OF THE DIFFERENTIAL DECAY RATE

Recently, a systematic framework has been developed [2–4] that enables us to compute the differential decay rates in the shape-function region. A series of matching calculations  $\text{QCD} \rightarrow \text{SCET} \rightarrow \text{HQET}$  is necessary to disentangle physics at the three different energy scales  $m_b$ ,  $\sqrt{m_b \Lambda_{\text{QCD}}}$ , and  $\Lambda_{\text{QCD}}$ . The general methodology is schematically visualized in Figure 2.

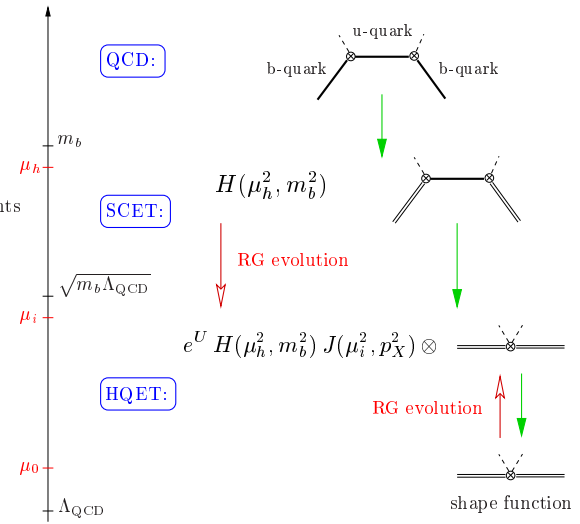


Figure 2. Contributions from different energy scales are factorized by matching onto Effective Field Theories:  $\text{QCD} \rightarrow \text{SCET} \rightarrow \text{HQET}$ .

The idea is as follows: Under the assumption of quark-hadron duality, the inclusive decay rate can be calculated in QCD using the optical theorem. The intermediate line denotes the energetic  $u$ -quark propagator. At a hard scale  $\mu_h \sim m_b$ , the amplitude is matched onto SCET, which correctly describes the infra-red degrees of freedom below this scale. Physics effects from scales above  $\mu_h$  are contained in a hard coefficient function  $H(\mu_h, m_b)$ . Since the  $u$ -quark momentum is parametrically off-shell by an amount of  $O(m_b \Lambda_{\text{QCD}})$ , the corresponding propagator can be integrated out at an intermediate matching scale  $\mu_i \sim \sqrt{m_b \Lambda_{\text{QCD}}}$ , leading to a perturbatively calculable jet function  $J$  and a low-energy description in HQET. The matrix element of the resulting leading power operator defines the hadronic shape function, which cannot be computed using analytic techniques. Large (Sudakov) logarithms are resummed when evolving the hard function from the hard scale  $\mu_h$  down to the intermediate scale  $\mu_i$ . Finally the decay amplitude is expressed as a convolution integral of perturbatively calculable functions and the shape function renormalized at  $\mu_i$ .

Event fractions and spectra are derived by performing the necessary phase-space integrations, *before* integrating over the shape function. In this way, the results are model independent and once again given as convolution integrals over the shape function.

### 3. PROPERTIES OF THE SHAPE FUNCTION

The shape function is a non-perturbative structure function that encodes the Fermi motion of the heavy quark inside the  $B$  meson [10]. Although the functional form of it cannot be derived using analytical techniques, it is nevertheless possible to study other properties of it using perturbation theory. In particular, the dependence on the renormalization scale  $\mu$  can be reliably computed as long as  $\mu$  is much larger than  $\Lambda_{\text{QCD}}$ . At leading order in renormalization-group improved perturbation theory it is given by the simple formula (for  $\mu_i \geq \mu_0$ )

$$\hat{S}(\hat{\omega}, \mu_i) = \frac{e^{V_S(\mu_i, \mu_0)}}{\Gamma(\eta)} \int_0^{\hat{\omega}} d\hat{\omega}' \frac{\hat{S}(\hat{\omega}', \mu_0)}{\mu_0^\eta (\hat{\omega} - \hat{\omega}')^{1-\eta}}, \quad (2)$$

where  $\eta = (16/25) \ln(\alpha_s(\mu_0)/\alpha_s(\mu_i))$ , and the exponent  $V_S$  vanishes in the limit  $\mu_i \rightarrow \mu_0$ . (The hatted notation denotes that the shape function is defined in a scheme-independent way and has support for  $\hat{\omega} \in [0, \infty[$ . For details, see Ref. [3].) As a consequence of (2), radiative corrections build up a tail that vanishes slower than  $\hat{\omega}^{-1}$  for  $\hat{\omega} \rightarrow \infty$ . This means that moments of the shape function (including its norm) are UV-divergent. This is, however, not an obstacle in practice, where the shape function is only needed over a finite interval. It is then natural to define moments accordingly over a finite integration domain, by means of a cutoff. Expanding them in a local OPE allows us to extract information about the shape function from the measurement of HQET parameters such as  $\bar{\Lambda}$  and  $\mu_\pi^2$ . The shape-function mass scheme [3] is convenient for such calculations and free of renormalon ambiguities. We stress, however, that information of  $\bar{\Lambda}$  and  $\mu_\pi^2$  in *any* low-scale subtracted mass scheme is useful, since there exist perturbatively calculable relations between these mass definitions.

A somewhat surprising observation is made by inspecting the behaviour of the moments under variation of the cutoff. It turns out that their values *decrease* for larger cutoffs. It follows that the tail of the shape function must be negative! In fact, it is possible to derive the explicit form of the shape function itself for large values of  $\hat{\omega} \gg \Lambda_{\text{QCD}}$ . We find that the asymptotic tail is given in the  $\overline{\text{MS}}$  scheme as [3]

$$\hat{S}(\hat{\omega}, \mu) \xrightarrow{\hat{\omega} \gg \Lambda_{\text{QCD}}} -\frac{C_F \alpha_s(\mu)}{\pi} \frac{1}{\hat{\omega} - \bar{\Lambda}} \times \left( 2 \ln \frac{\hat{\omega} - \bar{\Lambda}}{\mu} + 1 \right) + \dots, \quad (3)$$

and one has to drop the common interpretation of the renormalized shape function as a probability distribution.

#### 3.1. MODEL SHAPE FUNCTIONS

In the region  $\hat{\omega} \sim \Lambda_{\text{QCD}}$ , where it is relevant for phenomenological applications, the shape function cannot be computed within perturbation theory. In the following we will use a simple model that is consistent with all analytic constraints mentioned above. The model is constructed in such a way that its first few moments are consistent with the experimental values  $\bar{\Lambda} = (0.63 \pm 0.07)$  GeV and  $\mu_\pi^2 = (0.27 \pm 0.07)$  GeV $^2$  at a reference scale of  $\mu_i = 1.5$  GeV in the shape-function scheme (see Ref. [3] and references therein). Below we will use nine different functions (corresponding to the nine different pairs of values  $(\bar{\Lambda}, \mu_\pi^2)$  when varied within their errors) to account for our ignorance of the functional form

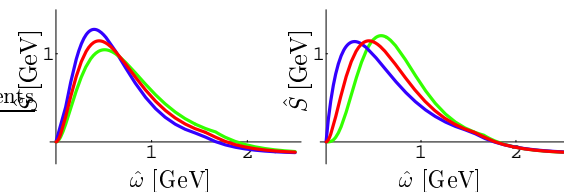


Figure 3. Model shape function under variation of the numerical values for  $\bar{\Lambda}$  and  $\mu_\pi^2$  within their errors. Correlated variations are shown on the left, anti-correlated on the right.

of the shape function. Figure 3 is intended to give the reader an idea of such variations. We stress, however, that a hypothetical knowledge of the first few moments to arbitrary precision would not determine the functional form of the shape function.

#### 4. EVENT FRACTIONS WITH CUTS ON $P_+$ OR $M_X$

With the methodology outlined in Section 2 we find the following expression for the fraction of events that survive a cut  $P_+ \leq \Delta_P$ , i. e. that are located below a horizontal line in the phase-space picture in Figure 1. At leading power in  $\Lambda_{\text{QCD}}/M_B$  and at next-to-leading order in renormalization-group improved perturbation theory, it is given as a weighted integral over the shape function:

$$F_P(\Delta_P) = T(a) e^{V_H(\mu_h, \mu_i)} \times \int_0^{\Delta_P} d\hat{\omega} \hat{S}(\hat{\omega}, \mu_i) W_P(\hat{\omega}, \Delta_P, a). \quad (4)$$

Large Sudakov logarithms are resummed in the expression  $T(a) e^{V_H(\mu_h, \mu_i)}$  (where  $a = 16/25 \times \ln(\alpha_s(\mu_i)/\alpha_s(\mu_h)) \approx 0.3$  for typical choices of  $\mu_h, \mu_i$ ), and the weight function  $W_P$  is perturbatively calculable [3] and starts as  $W_P = 1 + O(\alpha_s)$ .

When cutting on the hadronic invariant mass  $M_X^2 \leq s_0$  instead, the corresponding event fraction is given by

$$F_M(s_0) = F_P(s_0/M_B) + T(a) e^{V_H(\mu_h, \mu_i)} \times \int_{\sqrt{s_0}}^{\infty} d\hat{\omega} \hat{S}(\hat{\omega}, \mu_i) W_{\text{triangle}}(\hat{\omega}). \quad (5)$$

The two terms in the above expression can be easily interpreted using the phase-space picture in Figure 1. For an optimal cut  $s_0 = M_D^2$  the allowed region (dark gray) splits into two distinct areas, separated by the dashed line. Events below that line are included in the count by the first term in (5). The second term counts events in the triangle-shaped region above the dashed line. To account for the tip of this triangle ( $P_+ = P_- = \sqrt{s_0}$ ) is problematic in the

aforementioned framework, because the assumption  $P_+ \ll P_-$  and the resulting power-expansion rules are no longer valid. However, only few events are located near the tip, which is reflected in the finding that the corresponding contribution to  $F_M$  scales like  $(\Lambda_{\text{QCD}}/M_B)^{(3-a)/2}$  (assuming  $s_0 \sim \Lambda_{\text{QCD}} M_B$ ). Therefore one obtains a well defined leading power expression by setting the upper limit of integration from  $\sqrt{s_0}$  to  $\infty$  [3]. It is unclear, however, how to treat power corrections to  $F_M$  systematically in the future improvement of this result.

#### 4.1. MODEL-INDEPENDENT RELATIONS

QCD-Factorization is a powerful tool because the non-perturbative structure functions entering the theoretical description are universal, process-independent quantities. The shape function needed in this discussion on  $B \rightarrow X_u l^- \bar{\nu}$  decays is also the only leading-power structure function entering the calculation of the important  $B \rightarrow X_s \gamma$  decay rate. In fact, at leading power and leading order in  $\alpha_s$ , the shape function is identical to the photon spectrum. This implies that it is possible to construct relations between the photon spectrum and the event distribution functions in  $B \rightarrow X_u l^- \bar{\nu}$  decays in which the shape function has been eliminated. An example of such a relation is [4]

$$F_P(\Delta) = \int_{\frac{M_B}{2} - \Delta}^{\frac{M_B}{2}} dE_\gamma \frac{1}{\Gamma_s} \frac{d\Gamma_s}{dE_\gamma} \underbrace{w(\Delta, E_\gamma)}_{1 + \alpha_s \ln \dots}. \quad (6)$$

The weight function  $w$  is perturbatively calculable once our formalism has been applied to calculate the  $B \rightarrow X_s \gamma$  photon spectrum. Note that a similar relation to the hadronic invariant mass distribution  $F_M$  would be possible, but more complicated. Because of the contribution from the triangle region, the photon spectrum would be needed over a larger window and beyond the region where it is experimentally known with acceptable precision.

#### 4.2. MODEL PREDICTIONS

We use the nine model shape functions discussed in Section 3.1 to predict the event fractions

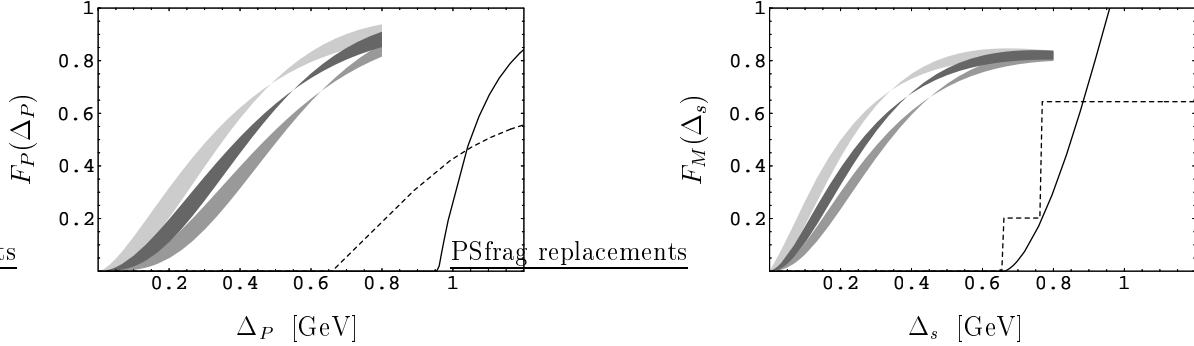


Figure 4. Model Predictions for  $F_P(\Delta_P)$  and  $F_M(\Delta_s)$  with  $\Delta_s = s_0/M_B$ . Each gray band corresponds to a fixed value of  $\bar{\Lambda}(\mu_i, \mu_i)$ , while the value of  $\mu_\pi^2(\mu_i, \mu_i)$  is varied within its error bars. The solid lines on the right in each graph denote the inclusive  $B \rightarrow X_c$  background, while the dashed lines indicate exclusive  $B \rightarrow D^{(*)}$  decays.

$F_P$  and  $F_M$  and demonstrate their sensitivity to the shape function. In principle, one also has to vary the functional form of the shape function without violating the constraints for its first few moments. In the end we find, however, that such variations are already covered in the sample of the nine models [3].

In Figure 4 our results are depicted as gray bands. Each of the bands represents the results using shape function models that correspond to a fixed value of  $\bar{\Lambda}$ , while the numerical value of  $\mu_\pi^2$  is varied within its error bars. We draw three bands for three values of  $\bar{\Lambda}$ : 0.56 GeV, 0.63 GeV, and 0.70 GeV, in accordance with our discussion in Section 3.1. The calculations are valid for  $\Delta_P$  and  $\Delta_s = s_0/M_B$  of order  $\Lambda_{\text{QCD}}$ . If these values are too small, i. e. parametrically of order  $\Lambda_{\text{QCD}}^2/M_B \approx 50$  MeV, the assumption of quark-hadron duality is no longer justified. If, on the other hand,  $\Delta_{P,s}$  are larger than about 0.8 GeV, the collinear expansion used in the calculation breaks down.

Our findings are summarized in Table 1 below. For “ideal” cuts, i. e. where the charm background starts,  $\Delta_{P,s} = M_D^2/M_B \approx 660$  MeV. The results show that cutting on the hadronic invariant mass  $M_X \leq M_D$  is rather insensitive to shape-function effects. However, due to detector

resolution effects, it is typically necessary to lower the cut and move away from the point where the charm background starts. In that case, the uncertainties due to our ignorance of the shape function become quickly larger, and are of comparable size to the uncertainties in an “ideal”  $P_+$  cut. It seems a clear advantage for cutting on hadronic invariant mass. However, we will argue below that it might not be necessary to move too far away from the charm background when cutting on  $P_+$ . In that case the hadronic invariant mass cut does not offer that advantage anymore and both methods give high efficiencies of about 70-80% with a relative uncertainty of roughly 10%.

Table 1  
Shape-function uncertainties for typical cuts on the hadronic variables  $M_X$  and  $P_+$ .

Cut	Efficiency
$M_X \leq M_D$	$(81.4^{+3.2}_{-3.7})\%$
$M_X \leq (1.7 \text{ GeV})$	$(78.2^{+4.9}_{-5.2})\%$
$M_X \leq (1.55 \text{ GeV})$	$(72.7^{+6.4}_{-6.3})\%$
$P_+ \leq \frac{M_D^2}{M_B} = 0.66 \text{ GeV}$	$(79.6^{+8.2}_{-8.2})\%$
$P_+ \leq 0.55 \text{ GeV}$	$(69.0^{+9.7}_{-12.1})\%$

## 5. CUTTING ON THE CHARGED LEPTON ENERGY

A prominent alternative way to discriminate the charm background is to cut on the charged-lepton energy. This is experimentally favored because it does not require the reconstruction of the neutrino momentum. (Both cutting on  $P_+$  or  $M_X$  need a neutrino reconstruction.) Unfortunately, the method is not favored by theorists, for several reasons. The most obvious one is that far fewer events survive such a cut. In our prediction this is reflected by the fact that the weight function is suppressed by a power of  $\Lambda_{\text{QCD}}/M_B$ :

$$F_E(\Delta_E) = T(a) e^{V_H(\mu_h, \mu_i)} \times \int_0^{\Delta_E} d\hat{\omega} \hat{S}(\hat{\omega}, \mu_i) \frac{2(\Delta_E - \hat{\omega})}{M_B - \hat{\omega}} [1 + O(\alpha_s)], \quad (7)$$

where  $\Delta_E = M_B - 2E_0$  and  $E_0$  is the lower limit of allowed lepton energy. Because of the rather low efficiency, this method is more prone to uncertainties from other effects, e.g. weak annihilation [11].

Numerical predictions using shape-function models are visualized in Figure 5 and summarized in Table 2. For orientation, the beginning of the charm background at  $\Delta_E = 660$  MeV is marked with an arrow in the Figure. Evidently, the relative shape-function uncertainties are large, and do not show a “focusing effect” as in the case of  $P_+$  or  $M_X$  cuts. Because of the large shape-function sensitivity and the overall small efficiency, the extraction of  $|V_{ub}|$  from

Table 2

Predictions and shape-function uncertainties for a cut on the charged lepton energy. For comparison, the results using the DeFazio/Neubert (DFN) model [12] are also given.

cut	$E_0$ [GeV]	$\Delta_E$ [GeV]	DFN [%]	BLNP [%]
$E_l \geq 2.31$	0.66	$7.9^{+3.4}_{-2.2}$	$12.5^{+3.4}_{-3.5}$	
$E_l \geq 2.2$	0.88	$14.4^{+4.4}_{-3.3}$	$22.2^{+3.2}_{-3.6}$	
$E_l \geq 2.1$	1.08	$20.9^{+4.9}_{-4.1}$	$31.7^{+3.0}_{-3.1}$	

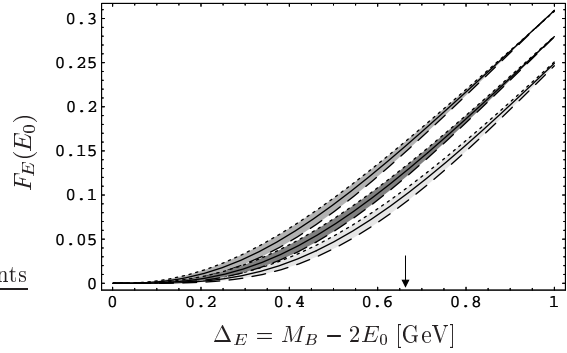


Figure 5. Model Predictions for the event fraction  $F_E$ . The bands are explained in Figure 4, and the arrow indicates the start of the charm background.

the charged-lepton energy endpoint region is theoretically disfavored.

An interesting observation can be made when comparing the third column in Table 2 with our results (BLNP = Bosch, Lange, Neubert, Paz [3]) in the fourth column. The former are predictions using the familiar DeFazio/Neubert model (DFN) of Ref. [12], where a simple replacement rule is used to implement the shape function into the results of parton-level calculations. The crucial difference is that our framework allows for a clean separation of short- and long-distance physics effects. In order to demonstrate this, consider the one-loop order result of the triple differential decay rate [2,3,12]. The leading logarithm comes with a coefficient of  $-4$ . In the framework of factorization, this coefficient will split into  $-4 = -8 + 4$ . While the leading logarithm of the jet function comes with the coefficient  $+4$ , the  $-8$  will be absorbed in the “partonic” shape function. The simple replacement rule of the DFN model does not capture this effect correctly. In addition to this important observation, the factorization framework allows for a systematic Sudakov resummation, which was not performed in the work of [12].

The numerical impact of these improvements over our previous understanding is that the predictions for the event fractions in the charged-

lepton energy endpoint have increased quite noticeably. This implies in turn that experimental  $|V_{ub}|$  determinations from the charged-lepton energy endpoint region might need to be corrected to lower values. In general, our analysis for  $B \rightarrow X_u l^- \bar{\nu}$  decay spectra in the shape-function region suggests that more events than previously anticipated are located in the shape-function region. It will be most interesting to study how power corrections will affect this conclusion.

## 6. CHARM BACKGROUND

The  $P_+$  spectrum has a considerable advantage over the hadronic-mass spectrum when considering the charm background. It is straightforward to visualize the area in phase space that is populated by inclusive  $B \rightarrow X_c$  decays. The OPE prediction uses quark-hadron duality and the fact that  $p_+ p_- \geq m_c^2$  in the parton picture. Here,  $p_{\pm} = P_{\pm} - \bar{\Lambda}$  are the light-cone components of the parton momentum, and  $m_c$  is the charm quark mass. The dotted line in Figure 6 marks the threshold  $p_+ p_- = p^2 = m_c^2$ . At tree-level, all events are located on that line. Radiative corrections smear the event distribution into the area above it. In this sense, the tree-level scenario serves as an upper bound of the inclusive charm background. Note that the dotted line touches the tip of the triangle,  $P_+ = P_- = M_D$  and extends to the right while always staying above the exclusive  $B \rightarrow D$  solid line. It follows that the variable  $P_+$  is bound to be always greater than approximately 960 MeV in the parton model. Therefore an ideal cut on  $P_+ = 660$  MeV has the advantage of a comfortable “buffer zone” to the inclusive background.

The gap between the charm-free area (dark gray) and the inclusive charm background (above the dotted line) is filled with exclusive final states such as  $B \rightarrow D$ ,  $B \rightarrow D^*$ ,  $B \rightarrow D\pi$ , etc.

In Figure 4 the results for a tree-level calculation [4] of the inclusive and exclusive event fractions are drawn as solid and short-dashed lines, respectively. Note that the event fractions are normalized to unity; however, the reader should keep in mind that the  $B \rightarrow X_c$  background is about 60 times larger than the  $B \rightarrow X_u$  signal.

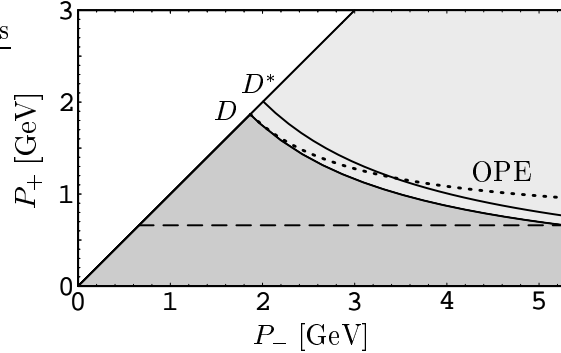


Figure 6. Phase-space picture for the charm background. The exclusive  $B \rightarrow D$  events are located on the lower solid line. The OPE prediction for inclusive  $B \rightarrow X_c$  events are located above the dashed line. The gap is filled with exclusive events  $B \rightarrow D^*$ ,  $B \rightarrow D\pi$ , etc.

Consider now what happens when the quantities  $\Delta_{P,s}$  approach the charm threshold near 660 MeV. The charmed hadronic invariant mass spectrum receives step increments when the  $D$  and  $D^*$  phase space becomes available. At the same time, the inclusive rates start near 660 MeV and reaches unity at 960 MeV in the tree approximation. Detector resolution effects smear the charm events into the region below 660 MeV, and force us to move away from the ideal cut, which leads to enhanced shape-function uncertainties in the  $B \rightarrow X_u$  event fractions (see Table 1).

The scenario for the  $P_+$  spectrum is different. The short-dashed line in the left part of Figure 4 also starts near 660 MeV, but has a smooth onset. The same applies when the  $D^*$  phase space becomes available, leading to a (tiny) kink in the line. However, up until this point, the charm background consists *exclusively* of  $B \rightarrow D$  events, since the inclusive events start much later at 960 MeV. The knowledge of the precise nature of the background ought to help experimentally to stay closer to the ideal cut, because it can be modeled with greater precision. We believe that this fact, together with the cleanliness of the theoretical description, make the  $P_+$  method an excellent high-efficiency candidate for a determination of

$|V_{ub}|$ , and we urge the experimental community to perform a measurement of the  $P_+$  spectrum.

## 7. CONCLUSION

In this talk we have presented recent advances in the understanding of inclusive  $B$  decays in the shape-function region. Using effective field theory techniques, a systematic framework was developed, where a simple OPE cannot be used due to soft shape function effects. New results for event distributions of several important kinematic quantities, including the hadronic invariant mass and the charged-lepton energy, have been presented. We advertised a new method for the extraction of  $|V_{ub}|$  based on the  $P_+$  spectrum. We stress, however, that this should not be understood as a discouragement of pursuing other methods, but rather as an encouragement to consider the  $P_+$  method as a powerful alternative.

The calculations have been performed in the heavy-quark limit and at next-to-leading order in RG-improved perturbation theory. Our prediction for the fraction of events with the optimal cut  $P_+ \leq M_D^2/M_B$  is [4]

$$F_P = (79.6 \pm 10.8 \pm 6.2 \pm 8.0)\%, \quad (8)$$

where the errors represent the sensitivity to the shape function, an estimate of  $\mathcal{O}(\alpha_s^2)$  contributions, and power corrections, respectively. Each of these uncertainties can be reduced in the future within the general framework presented in [2–4] and outlined in Section 2. Much can be learned about the shape function from the  $B \rightarrow X_s \gamma$  photon spectrum, once the formalism has been applied. The calculation of  $\mathcal{O}(\alpha_s^2)$  corrections would be a major effort, but is feasible in the future. The important question of power corrections are currently investigated by several groups in the theory community.

The CKM-matrix element  $|V_{ub}|$  can be extracted by comparing a measurement of the partial rate  $\Gamma_u(P_+ \leq \Delta_P)$  with a theoretical prediction for the product of the event fraction  $F_P(\Delta_P)$  and the total inclusive  $\bar{B} \rightarrow X_u l^- \bar{\nu}$  rate. The resulting theoretical uncertainty on  $|V_{ub}|$  is

$$\frac{\delta|V_{ub}|}{|V_{ub}|} = (\pm 7 \pm 4 \pm 5 \pm 4)\%, \quad (9)$$

where the last error comes from the uncertainty in the total rate [13,14]. Because of the large efficiency of the  $P_+$  cut, weak annihilation effects [11] have an influence on  $|V_{ub}|$  of less than 2% and can be safely neglected.

## ACKNOWLEDGMENTS

It is a pleasure to acknowledge my collaborators Stefan Bosch, Matthias Neubert, and Gil Paz. I would also like to thank Jon Rosner for inviting me to give this talk, and the organizers of BEACH 2004 for a beautiful conference. This research was supported by the National Science Foundation under Grant PHY-0098631.

## REFERENCES

1. M. Battaglia and L. Gibbons, [PDG Collaboration], *Phys. Lett. B* **592**, 1 (2004).
2. C. W. Bauer and A. V. Manohar, hep-ph/0312109.
3. S. W. Bosch, B. O. Lange, M. Neubert and G. Paz, hep-ph/0402094.
4. S. W. Bosch, B. O. Lange, M. Neubert and G. Paz, hep-ph/0403223.
5. C. W. Bauer, S. Fleming and M. E. Luke, *Phys. Rev. D* **63**, 014006 (2001).
6. C. W. Bauer, S. Fleming, D. Pirjol and I. W. Stewart, *Phys. Rev. D* **63**, 114020 (2001).
7. C. W. Bauer, D. Pirjol and I. W. Stewart, *Phys. Rev. D* **65**, 054022 (2002).
8. For a review, see M. Neubert, *Phys. Rept.* **245**, 259 (1994).
9. B. O. Lange and M. Neubert, *Phys. Rev. Lett.* **91**, 102001 (2003).
10. M. Neubert, *Phys. Rev. D* **49**, 3392 (1994); *Phys. Rev. D* **49**, 4623 (1994).
11. M. B. Voloshin, *Phys. Lett. B* **515**, 74 (2001).
12. F. De Fazio and M. Neubert, *JHEP* **9906**, 017 (1999).
13. A. H. Hoang, Z. Ligeti and A. V. Manohar, *Phys. Rev. Lett.* **82**, 277 (1999).
14. N. Uraltsev, *Int. J. Mod. Phys. A* **14**, 4641 (1999).